

Semi-Supervised Contrastive Learning for Remote Sensing: Identifying Ancient Urbanization in the South Central Andes

Jiachen Xu,¹ James Zimmer-Dauphinee,² Quan Liu,³ Yuxuan Shi,¹ Steven Wernke,² Yuankai Huo³

¹ School of Engineering, Vanderbilt University

² Department of Anthropology, Vanderbilt University

³ Department of Electrical Engineering and Computer Science, Vanderbilt University

Contact author: yuankai.huo@vanderbilt.edu

Abstract

The detection of ancient settlements is a key focus in landscape archaeology. Traditionally, settlements were identified through pedestrian survey, as researchers physically traversed the landscape and recorded settlement locations. Recently the manual identification and labeling of ancient remains in satellite imagery have increased the scale of archaeological data collection, but the process remains tremendously time-consuming and arduous. The development of self-supervised learning (e.g., contrastive learning) offers a scalable learning scheme in locating archaeological sites using unlabeled satellite and historical aerial images. However, archaeology sites are only present in a very small proportion of the whole landscape, while the modern contrastive-supervised learning approach typically yield inferior performance on the highly balanced dataset, such as identifying sparsely localized ancient urbanization on a large area using satellite images. In this work, we propose a framework to solve this long-tail problem. As opposed to the existing contrastive learning approaches that typically treat the labeled and unlabeled data separately, the proposed method reforms the learning paradigm under a semi-supervised setting to fully utilize the precious annotated data (<7% in our setting). Specifically, the highly unbalanced nature of the data is employed as the prior knowledge to form pseudo negative pairs by ranking the similarities between unannotated image patches and annotated anchor images. In this study, we used 95,358 unlabeled images and 5,830 labeled images to solve the problem of detecting ancient buildings from a long-tailed satellite image dataset. From the results, our semi-supervised contrastive learning model achieved a promising testing balanced accuracy of 79.0%, which is 3.8% improvement over state-of-the-art approaches.

Introduction

Archaeological structures and settlements are essential primary sources for archaeologists to study the economic, political, and social systems of ancient civilizations. Traditional approaches of discovering archaic sites were field-based survey methods, requiring professionals to physically examine the landscape for evidence of ancient material culture. Since the early 2000s, archaeologists began to make use of

satellite and historical aerial images to understand the spatial and structural patterns of archaeological features in the images, which significantly upscaled survey coverage compared to traditional field-based methods (Hanson and Oltean 2012; Fowler 2002; Lasaponara and Masini 2012). Nonetheless, due to the sparse distribution of archaeological features on the landscape, manual identification and labeling of ancient remains in satellite imagery can be tremendously time-consuming and arduous, resulting in huge datasets with few labels (Mnih and Hinton 2012). It has been a long standing learning challenge in remote sensing, which is to develop a effective machine learning algorithm on such large-scale, sparsely annotated, and highly unbalanced data, so as to automate the resource extensive information extraction procedures.

Over recent years, the rapid development of self-supervised contrastive learning has provided an appealing direction to utilize large-scale sparsely annotated data. However, the proportion of images containing archaic sites is often relatively low (<7% in our setting). Such unbalanced data distribution is problematic for modern contrastive learning algorithms (Chen and He 2021; Grill et al. 2020), which might lead to excessive favoring representations for the majority classes. By reforming the contrastive learning in a semi-supervised setting, we emphasize the critical role of the precious annotated positive instances in both training and fine-tuning stages.

In this work, we propose a novel self-supervised contrastive learning framework to identify ancient urbanization in the south central Andes. As opposed to the existing self-supervised learning approaches that typically model the labeled and unlabeled data separately, we introduce a holistic end-to-end semi-supervised learning framework that utilizes the highly unbalanced nature of the data to form pseudo negative pairs by ranking the similarities between unannotated image patches and annotated anchor images. Specifically, pseudo negative images are employed to calculate a supervised contrastive (SupCon) loss (Khosla et al. 2020), which is seamlessly integrated with the contrastive loss (Chen et al. 2020). To our knowledge, this is the first study of investigating semi-supervised contrastive learning in discovering ancient remains from aerial satellite images.

This project surveys an approximately 4000 km² region of the western cordillera of the southern Peruvian Andes.

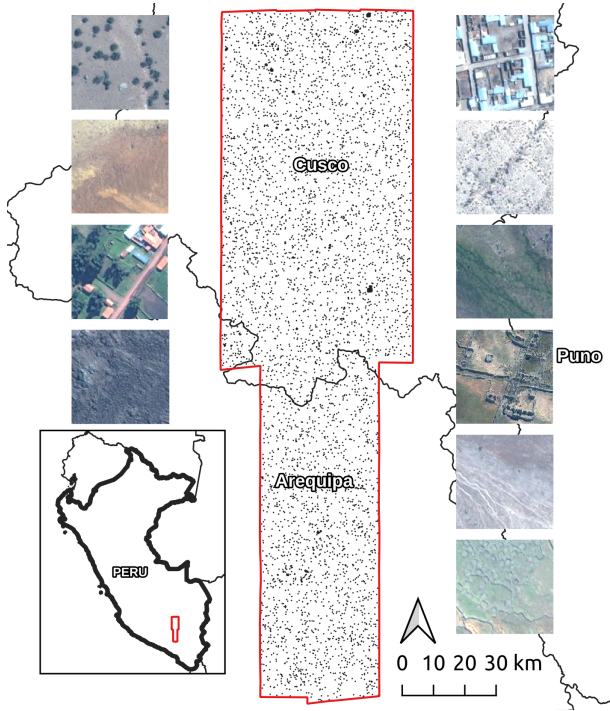


Figure 1: Survey Region. The study region encompasses approximately 4000 km² of the western cordillera of the southern Peruvian highlands, including portions of the modern Cusco and Arequipa districts. Sample tiles represent the diversity of land formation in the region and sample locations are shown in black.

Due to the arid environment and limited vegetation coverage of this region, satellites are capable of capturing clear and unobscured images of the ground and archaeological features of interest. In addition, ancient structures were primarily constructed from stone, leading to relatively good preservation and therefore high visibility in satellite imagery. Nonetheless, the construction materials are comprised nearly entirely of the same materials as the background matrix (local rock and soil), making traditional spectral remote sensing techniques ineffective (Casana 2014). The overview of the study region is shown in Figure 1.

Utilizing images taken by Worldview 2 and Worldview 3 Satellite constellations, our dataset consists of 95358 unlabeled images and 5830 labeled images, where the ratio between positive and negative instances is roughly 1:100. We show that our semi-supervised contrastive learning model outperforms its self-supervised and fully-supervised counterparts, along with traditional supervised networks like ResNet50.

In summary, the contributions of this paper are:

- We present a semi-supervised contrastive training framework that effectively learns from large-scale, sparsely annotated, and highly unbalanced remote sensing data.
- The highly unbalanced nature of the data is employed as the prior knowledge to form pseudo negative pairs by rank-

ing the similarities between unannotated image patches and annotated anchor images.

- To our knowledge, this is the first study that investigates semi-supervised contrastive learning in discovering ancient remains from aerial satellite images.

Related Works

Contrastive Representation Learning

In contrast to supervised learning (Cunningham, Cord, and Delany 2008) that requires the presence of labeled inputs to predict outputs, self-supervised learning (Le 2013) refers to the identification of the hidden patterns of a dataset without the usage of any labels. As a relatively new family of self-supervised learning, contrastive representation learning has recently become a prominent approach in solving various computer vision tasks with state-of-the-art performance (Wu et al. 2018; Noroozi and Favaro 2016; Zhuang, Zhai, and Yamins 2019; Hjelm et al. 2018; Chuang et al. 2020; Tian et al. 2020; Khosla et al. 2020; Cui et al. 2021). Designed to learn the general features of large datasets without labels, contrastive learning aims to pull similar sample pairs together while pushing dissimilar pairs far apart. As a result, the model is capable of learning the high-level features of a dataset even with few or no labels available.

Over the recent years, various contrastive representation learning methods have been proposed with different implementations. SimCLR (Chen et al. 2020) aims to pull the representations of images in the same class closer and minimize the similarity of images from different categories. SwAV (Caron et al. 2020) applies online clustering on different augmentations of the same image instead of performing explicit pairwise feature comparisons. Wu et al. (Wu et al. 2018) proposes the use of an offline memory bank to store all data representations, and training data will be randomly selected for negative pairs minimization. Instead of an offline dictionary, MoCo (He et al. 2020) utilizes a momentum design to build a dynamic dictionary that stores a negative sample pool, which demands a large batch size. To further alleviate the cost of storing negative pairs, BYOL (Grill et al. 2020) is proposed to incorporate an asynchronous momentum encoder into the model so that it can use only the positive pairs for training. Recently, SimSiam (Chen and He 2021) is designed to save GPU memory consumption via fully eliminating the momentum encoder.

Remote Sensing with Machine Learning

Remote sensing refers to the collection, processing, and interpretation of videos and imagery taken at a distance, often employing an overhead perspective (Campbell and Wynne 2011; Cracknell 2007; Gupta 2017; Schowengerdt 2006). Through the use of aerial (Feng, Liu, and Gong 2015; Everaerts et al. 2008; Salami, Barrado, and Pastor 2014; Nithammer et al. 2012; Pajares 2015; Matese et al. 2015) or satellite platforms (Ozesmi and Bauer 2002; Harris 1987; Tucker and Sellers 1986; Parcak 2009; Chuvieco 2020; Verbyla 1995), these images can cover great areas while recording information in both visible and non-visible bands of the electromagnetic spectrum, allowing the extraction of spatial

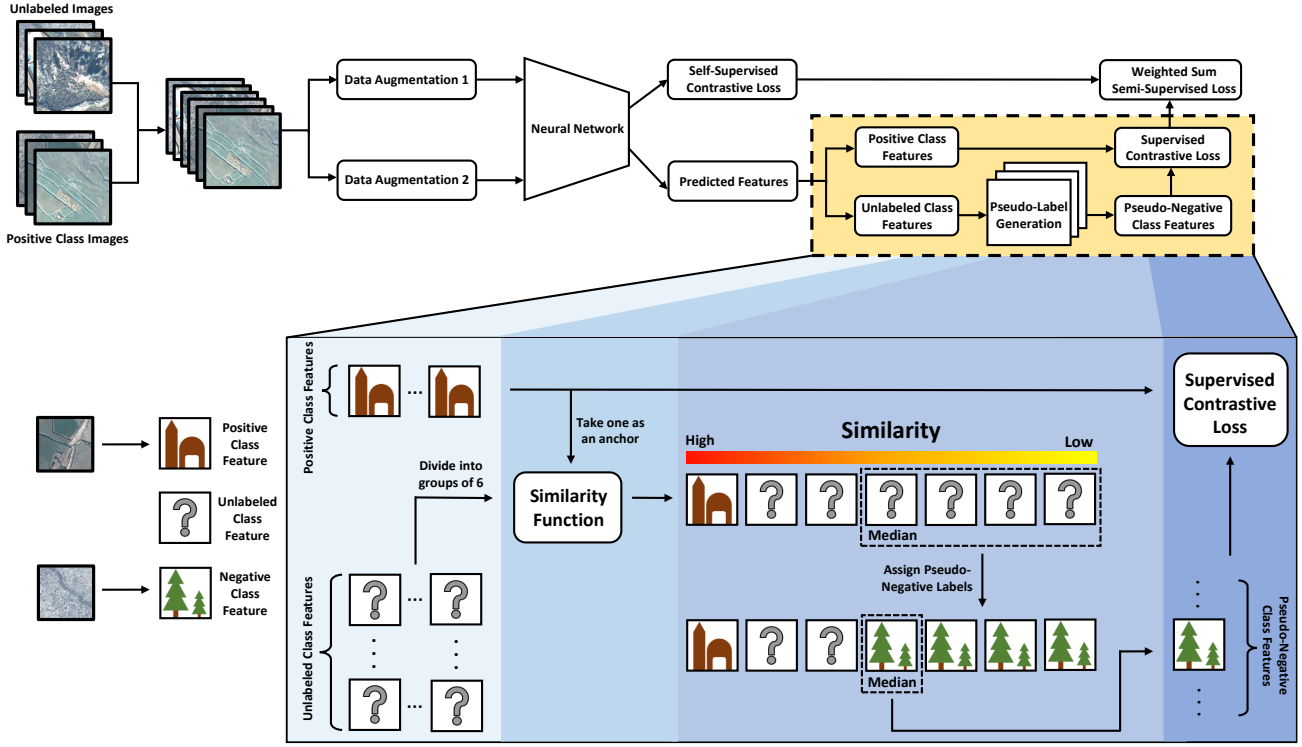


Figure 2: **Overall framework.** This figure demonstrates the general structure of our semi-supervised contrastive learning framework. The upper panel shows the general flow of our framework, which was adopted from the SimSiam network. The lower panel describes the process of obtaining the supervised contrastive loss from predicted features. The detailed discussions can be found in the Methods section.

patterns and information across large regions. Researchers can therefore widen their perspectives to study patterns that may otherwise be indistinguishable when data is only available at a local level.

Satellite remote sensing has contributed to the execution of a variety of tasks, including climate change measurement, crop condition monitoring, natural disaster alerts, and archaeological site detection (Harris 1987). Satellites were first introduced to the field of archaeology in the late 1900s, and the usage of satellite remote sensing in the detection of archaeological sites has developed rapidly ever since with constant incorporation of latest technologies. Entering the 2000s, the development of machine learning, specifically representation learning, offered major breakthroughs in the analytical approaches of satellite images, leading to seminal insights and discoveries in the field of archaeology (Lary et al. 2016; Camps-Valls 2009; Ali et al. 2015; Cooner, Shao, and Campbell 2016; Comer and Harrower 2013; Parcak 2019).

Methods

The overall design of our framework is demonstrated in Figure 2. The analysis of backbone network and pseudo-label synthesis is presented below.

Backbone Network

In this work, SimSiam is chosen as our backbone network due to its simplicity and effectiveness. Comparing to other widely-used self-supervised representation learning networks, SimSiam removes all additional structures like negative samples (SimCLR), momentum encoder (BYOL), or clustering (SwAV) yet still obtains great performance in learning representations of unlabeled datasets. A new compound loss is introduced to replace the SimSiam-embedded symmetric loss to integrate semi-supervised behaviors to the model. In addition, the recent mixed-precision training feature is utilized to accelerate the training process.

Pseudo-Label Synthesis

For the synthesis of pseudo-labels, a mixed array of unlabeled and positive class features is used as the starting point. The first step is to normalize this array. The array is decoupled into X features of unlabeled images (Group 1) and Y features of positively-labeled images (Group 2). Then, we divide the X unlabeled class features into subgroups of size k (16 in our case), and we end up with X/k subgroups. Meanwhile, a single feature is randomly selected from the Y positive class features for future use.

For each subgroup, we apply the cosine similarity function to compute the similarity between the previously se-

Algorithm 1: Pseudo-Code for generating pseudo negative pairs

```

# Input: An array of unlabeled class features:  $f_{un}$ 
# Input: An array of positive class features:  $f_{pos}$ 
# Output: An array of pseudo-negative class features:  $f_{neg}$ 

1:  $f_{un} = \text{Normalize}(f_{un})$ 
2:  $f_{pos} = \text{Normalize}(f_{pos})$ 
3: Divide  $f_{un}$  into groups of  $16 \rightarrow f_{un\_groups}$ 
4: Randomly choose a feature from  $f_{pos} \rightarrow f_{positive}$ 
5:  $f_{neg} = []$ 
6: for  $f_{un\_group}$  in  $f_{un\_groups}$  do
7:    $sim\_array = \text{Similarity\_Function}(f_{un\_group} + f_{positive})$ 
8:    $f_{neg}.append(\text{Median}(sim\_array))$ 
9: end for
10: return  $f_{neg}$ 

```

lected positive feature and the features in this subgroup. After that, the unlabeled image with the median similarity score is assigned a pseudo label (i.e., negative class) based on the hypothesis that the negative images dominate the distribution of the entire cohort. In this study, the ratio between positive and negative images is roughly 1:100.

The pseudo-code of generating such pseudo-label is presented in Algorithm 1. As an toy example, it assumes that there are 505 unlabeled images. Based on the ratio in this study, 500 of them should be negative and only 5 of them should be positive. Now, if the size of the batch is 16 and the images are randomly selected, the probability of having exactly n positive image(s) can be expressed as:

$$p(n) = \frac{\binom{5}{n} \cdot \binom{500}{16-n}}{\binom{505}{16}} \quad (1)$$

Then, the probability of having at most 1 positive image among the 16 selected samples is:

$$p(n \leq 1) = \sum_{n=0}^1 \frac{\binom{5}{n} \cdot \binom{500}{16-n}}{\binom{505}{16}} \approx 0.991 \quad (2)$$

Semi-supervised Contrastive Learning

The key innovation of our method is to propose a new semi-supervised contrastive learning strategy. In short, we aggregate the standard cosine similarity loss with the supervised SupCon loss. In each iteration of the training, X unlabeled images and Y positively-labeled images are utilized as inputs to our SimSiam model, and the generated symmetric loss is named $loss_cosine$. The formulas are defined as (Chen and He 2021):

$$\mathcal{D}(p_1, z_2) = -\frac{p_1}{\|p_1\|_2} \cdot \frac{z_2}{\|z_2\|_2} \quad (3)$$

$$\mathcal{L} = \frac{1}{2}\mathcal{D}(p_1, z_2) + \frac{1}{2}\mathcal{D}(p_2, z_1) \quad (4)$$

Then, the generated features mentioned in Backbone Network subsection is employed to calculate the supervised

loss, which is named $loss_super$. The features will go through the steps in the Pseudo-Label Synthesis subsection, and the products will be X/k pseudo-negative class features and Y positive class features (mentioned earlier in the subsection). Finally, those features are combined together as inputs to the SupCon (Khosla et al. 2020) loss function to calculate $loss_super$.

The formula for the SupCon loss is presented below (Khosla et al. 2020):

$$\begin{aligned} \mathcal{L}_{out}^{sup} &= \sum_{i \in I} \mathcal{L}_{out,i}^{sup} \\ &= \sum_{i \in I} \frac{-1}{|P(i)|} \sum_{p \in P(i)} \log \frac{\exp(z_i \cdot z_p / \tau)}{\sum_{a \in A(i)} \exp(z_i \cdot z_a / \tau)} \end{aligned} \quad (5)$$

As the final step, we aggregate $loss_cosine$ and $loss_super$ with a multi-task loss design that is inspired by Kendall (Kendall, Gal, and Cipolla 2018). This multi-task loss function is selected to eliminate the need for finding the relative weighting between multiple losses through fine-tuning parameters. The modified version of the formula is presented below:

Let v_1 and v_2 denote the two dynamic log variances, which serve the roles of weights (Kendall, Gal, and Cipolla 2018). Then, the total loss, denoted by $loss_{total}$, is calculated as:

$$loss_{total} = (e^{-v_1} \cdot loss_1 + v_1) + (e^{-v_2} \cdot loss_2 + v_2) \quad (6)$$

Data and Experiments

Data

The satellite images used in this analysis were collected by the WorldView 2 and WorldView 3 satellite constellations and were provided by the Digital Globe Foundation following color correction and orthographic correction using a coarse digital elevation model (DEM). The data was then pan-sharpened using the Bayesian fusion algorithm from Orfeo-Toolbox (Grizonnet et al. 2017) to increase the spatial resolution of the multi-spectral imagery to 0.5 m for the WorldView 2 imagery, and 0.3 m for the WorldView 3 imagery. In this study, all spatial bands were dropped except for the Red, Green, and Blue spectral bands, and the imagery was re-sampled from 32 bits to 8 bits to reduce the storage size and computational requirements. In total, those images covered approximately 4,000 km². Finally, the study region was divided into approximately 1.6 million image tiles of 76.8×76.8 meters (256×256 pixels at 0.3 m resolution).

5830 images were manually labeled, and 5000 of them were randomly selected. To balance the sample size for the sparsely distributed modern and ancient settlements on the landscape, an additional set of 830 images known to contain examples of archaeological or modern structures were added to provide additional representation of these categories. Since the ancient building were the objects of interests, all images were labeled into two classes: “ancient_building” (that is, “the presence of an archaeological structure,” defined as human-made structures less than 30 m

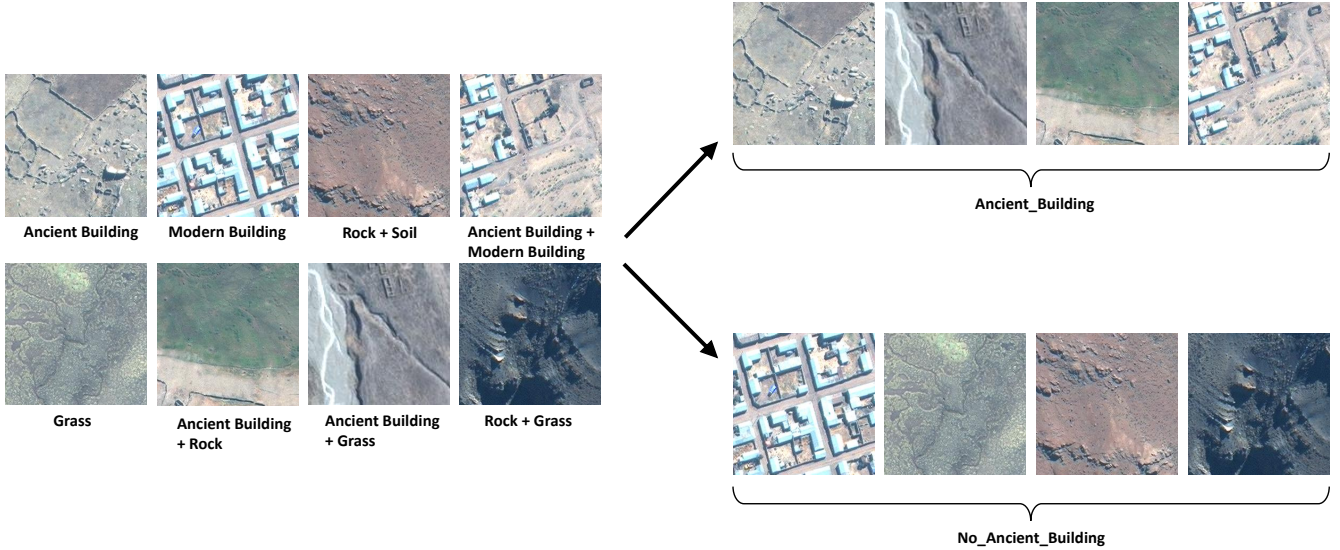


Figure 3: **Example of annotated classes.** This figure demonstrates example classes of the annotated data. The left panel shows the various types of unannotated images with a mixture of contents, including ancient/modern buildings, rock, soil, and grass. Due to the variety of potential objects, it’s unrealistic to create a separate class for each unique combination of objects. Therefore, two classes were created based on the presence of ancient buildings, which is shown in the right panel.

Dataset	# of Ancient_Building	# of No_Ancient_Building
Training	193 (Original)	4,272
	3,088 (Upsampled)	
Validation	65	610
Testing	71	619
Unannotated	95,358	

Table 1: Datasets Setup

in largest dimension without evidence of modern roofs or maintenance) and “no_ancient_building” (that is, “no presence of an archaeological structure”). From the remaining unlabeled images, around 100,000 images were randomly selected to train the self-supervised deep learning models. Finally, those images were visually examined, and the defective ones (missing data) were abandoned, resulting in an unlabeled dataset of 95,358 images. Sample images are presented in Figure 3.

Experimental Design

The 5830 labeled images were divided into training, validation, and testing splits, ensuring that images from the nearby physical space were placed into the same split to avoid the issue of data contamination. Additionally, in order to alleviate the unbalanced nature of our data source, the under-representative positive class (with ancient builds) in our training dataset were up-sampled to have the roughly equal distribution to the negative class. The details of the

data split are shown in Table 1. As the last step, all the labeled and unlabeled images were resized to 128×128 to expedite the training process.

Semi-Supervised Contrastive Training The proposed semi-supervised contrastive learning model was adopted from the SimSiam network with major modifications on the loss function. The optimizer used was SGD optimizer initialized with learning rate = 0.1, weight decay = 0.0001, and momentum = 0.9. The training dataset of unlabeled images had a batch size = 512, while the labeled dataset had a batch size = 16. The mixed-precision training features were integrated into our network to boost the training process. The model was trained for 200 epochs. The output for this model was a 2048 dimensional feature from the input images. All the training in this paper was conducted on a workstation with Intel Xeon Gold 5118 2.30 GHz CPU, 383 GB memory, and 2 NVIDIA GeForce RTX 2080 Ti GPU (11.0 GB dedicated GPU memory).

Backbone	Loss Function	Unlabeled Images	Labeled Images	F1 Score (macro)	Balanced Accuracy
ResNet50	Cross Entropy Loss	N/A	5,830	0.612	0.701
SimSiam	Loss 1	95,358	5,830	0.744	0.752
	Loss 1 + 2	95,358	5,830	0.762	0.790
	Loss 2	95,358	5,830	0.477	0.500

Table 2: Training Results



Figure 4: **Testing Sample Results** This figure presents representative samples from the testing results. The left panel indicates the true positive examples while the right panel indicates the true negative cases. Likewise, the upper row indicates the predicted positive ones while the lower row indicates the predicted negative ones.

Supervised Fine-tuning and Testing After pre-training the model using the unannotated data, an additional single linear layer was fine-tuned with labeled data. The F1 score and balanced accuracy on the validation set were used as the metrics to select the best performance epoch as well as the optimal hyper-parameters.

Results

Ablation Study

This ablation study consisted of two alternative versions of our pre-trained model: the first version conducted self-supervised contrastive learning using only `loss_cosine` discussed in the Methods section, inspired by the SimSiam network (Chen et al. 2020). By contrast, the second version conducted supervised contrastive learning using only `loss_super` discussed in the Methods section. The corresponding testing results have been presented in Table 2.

Comparison with Fully-Supervised Learning Benchmark

A fully supervised version of the training using only the labeled images was also established to further demonstrate the performance boost provided by unlabeled data. Since our self-supervised framework employed ResNet50 as the backbone model, it's also used here as the fully-supervised learning benchmark. SGD optimizer and cross entropy loss

were employed to create a standard training environment. The model was trained for 16 epochs. The trained model with the best validation performance was selected to run the testing dataset. The results were demonstrated in Table 2.

Discussion

In this study, we developed a new semi-supervised contrastive learning pseudo-label generation method based on similarity matrix with the ultimate goal of enhancing self-supervised training performance over highly unbalanced dataset. By integrating self-supervised and supervised loss functions, we designed a new learning framework that simultaneously learns from both the unannotated and the annotated data.

The conducted experiments had yielded promising results. In the ablation study, the model trained using only `loss_super` were relatively ineffective in identifying ancient buildings, while the model trained using only `loss_cosine` produced competitive F1 score and balanced accuracy, indicating that having a model pre-trained on unlabeled data using self-supervised contrastive learning was essential in distinguishing ancient buildings from other objects. Nonetheless, our proposed semi-supervised model trained with `loss_cosine + loss_super` outperformed its self-supervised and fully-supervised counterparts by a decent margin. This result showed that the integration of fully-supervised and

self-supervised networks offered complimentary properties. Furthermore, by comparing with the fully-supervised learning benchmarks (like ResNet50) with our model, our solution exhibited superior performance on unlabeled dataset.

Figure 4 offered additional insights into the performance of our framework. The upper left and lower right corners indicated the correct classes, while the remaining ones were either false positive or false negative. From the ablation study, the superior performance of our model could be attributed to the dynamic combination of fully-supervised and self-supervised information. The loss generated from the positive and pseudo-negative images served as an complement to the other loss functions that were generated solely on unlabeled instances.

Several potential improvements for our semi-supervised contrastive learning framework were as followed. First, our proposed pseudo-labeling strategy would only work for highly unbalanced data set. Moreover, the current model had not been extended to the multi-label classification scenarios. Meanwhile, the size of annotated training images in our study was still relatively small. To further facilitate the performance, we might need more training data, especially with more positive images (ancient building) from our predicted positive class.

Conclusion

In this project, we proposed a new semi-supervised contrastive learning method for identifying ancient urbanization in the South Central Andes from satellite imagery. As opposed to the existing solutions, we utilized the unbalanced nature of the large-scale unlabeled data to form pseudo negative pairs. Using such negative pairs, we leveraged the contrastive learning by introducing a holistic learning scheme with both cosine similarity loss and pseudo supervision loss functions. According to the experimental results, our proposed framework yielded superior accuracy and F1 score compared with its self-supervised and fully-supervised counterparts. The integrated model eventually outperformed traditional supervised networks (e.g., ResNet50) by 15% in F1 score and 8.9% in balanced accuracy.

Acknowledgements

This work has not been submitted for publication or presentation elsewhere.

References

Ali, I.; Greifeneder, F.; Stamenkovic, J.; Neumann, M.; and Notarnicola, C. 2015. Review of machine learning approaches for biomass and soil moisture retrievals from remote sensing data. *Remote Sensing*, 7(12): 16398–16421.

Campbell, J. B.; and Wynne, R. H. 2011. *Introduction to remote sensing*. Guilford Press.

Camps-Valls, G. 2009. Machine learning in remote sensing data processing. In *2009 IEEE international workshop on machine learning for signal processing*, 1–6. IEEE.

Caron, M.; Misra, I.; Mairal, J.; Goyal, P.; Bojanowski, P.; and Joulin, A. 2020. Unsupervised learning of visual fea-

tures by contrasting cluster assignments. *arXiv preprint arXiv:2006.09882*.

Casana, J. 2014. Regional-Scale Archaeological Remote Sensing in the Age of Big Data: Automated Site Discovery vs. Brute Force Methods. *Advances in Archaeological Practice*, 2(3): 222–233.

Chen, T.; Kornblith, S.; Norouzi, M.; and Hinton, G. 2020. A simple framework for contrastive learning of visual representations. In *International conference on machine learning*, 1597–1607. PMLR.

Chen, X.; and He, K. 2021. Exploring simple siamese representation learning. In *Proceedings of the IEEE/CVF Conference on Computer Vision and Pattern Recognition*, 15750–15758.

Chuang, C.-Y.; Robinson, J.; Yen-Chen, L.; Torralba, A.; and Jegelka, S. 2020. Debiased contrastive learning. *arXiv preprint arXiv:2007.00224*.

Chuvieco, E. 2020. *Fundamentals of satellite remote sensing: An environmental approach*. CRC press.

Comer, D. C.; and Harrower, M. J. 2013. *Mapping Archaeological Landscapes from Space*. SpringerBriefs in Archaeological Heritage Management. New York: Springer Science & Business Media. ISBN 978-1-4614-6074-9. Google-Books-ID: yWJDAAAQBAJ.

Cooner, A. J.; Shao, Y.; and Campbell, J. B. 2016. Detection of urban damage using remote sensing and machine learning algorithms: Revisiting the 2010 Haiti earthquake. *Remote Sensing*, 8(10): 868.

Cracknell, A. P. 2007. *Introduction to remote sensing*. CRC press.

Cui, J.; Zhong, Z.; Liu, S.; Yu, B.; and Jia, J. 2021. Parametric Contrastive Learning. *arXiv preprint arXiv:2107.12028*.

Cunningham, P.; Cord, M.; and Delany, S. J. 2008. Supervised learning. In *Machine learning techniques for multimedia*, 21–49. Springer.

Everaerts, J.; et al. 2008. The use of unmanned aerial vehicles (UAVs) for remote sensing and mapping. *The International Archives of the Photogrammetry, Remote Sensing and Spatial Information Sciences*, 37(2008): 1187–1192.

Feng, Q.; Liu, J.; and Gong, J. 2015. UAV remote sensing for urban vegetation mapping using random forest and texture analysis. *Remote sensing*, 7(1): 1074–1094.

Fowler, M. J. 2002. Satellite remote sensing and archaeology: a comparative study of satellite imagery of the environs of Figsbury Ring, Wiltshire. *Archaeological prospection*, 9(2): 55–69.

Grill, J.-B.; Strub, F.; Altché, F.; Tallec, C.; Richemond, P. H.; Buchatskaya, E.; Doersch, C.; Pires, B. A.; Guo, Z. D.; Azar, M. G.; et al. 2020. Bootstrap your own latent: A new approach to self-supervised learning. *arXiv preprint arXiv:2006.07733*.

Grizonnet, M.; Michel, J.; Poughon, V.; Inglada, J.; Savinaud, M.; and Cresson, R. 2017. Orfeo ToolBox: Open source processing of remote sensing images. *Open Geospatial Data, Software and Standards*, 2(1): 15.

Gupta, R. P. 2017. *Remote sensing geology*. Springer.

- Hanson, W. S.; and Oltean, I. A. 2012. *Archaeology from historical aerial and satellite archives*. Springer Science & Business Media.
- Harris, R. 1987. Satellite remote sensing. An introduction.
- He, K.; Fan, H.; Wu, Y.; Xie, S.; and Girshick, R. 2020. Momentum contrast for unsupervised visual representation learning. In *Proceedings of the IEEE/CVF Conference on Computer Vision and Pattern Recognition*, 9729–9738.
- Hjelm, R. D.; Fedorov, A.; Lavoie-Marchildon, S.; Grewal, K.; Bachman, P.; Trischler, A.; and Bengio, Y. 2018. Learning deep representations by mutual information estimation and maximization. *arXiv preprint arXiv:1808.06670*.
- Kendall, A.; Gal, Y.; and Cipolla, R. 2018. Multi-task learning using uncertainty to weigh losses for scene geometry and semantics. In *Proceedings of the IEEE conference on computer vision and pattern recognition*, 7482–7491.
- Khosla, P.; Teterwak, P.; Wang, C.; Sarna, A.; Tian, Y.; Isola, P.; Maschinot, A.; Liu, C.; and Krishnan, D. 2020. Supervised contrastive learning. *arXiv preprint arXiv:2004.11362*.
- Lary, D. J.; Alavi, A. H.; Gandomi, A. H.; and Walker, A. L. 2016. Machine learning in geosciences and remote sensing. *Geoscience Frontiers*, 7(1): 3–10.
- Lasaponara, R.; and Masini, N. 2012. *Satellite remote sensing: A new tool for archaeology*, volume 16. Springer Science & Business Media.
- Le, Q. V. 2013. Building high-level features using large scale unsupervised learning. In *2013 IEEE international conference on acoustics, speech and signal processing*, 8595–8598. IEEE.
- Matese, A.; Toscano, P.; Di Gennaro, S. F.; Genesio, L.; Vaccari, F. P.; Primicerio, J.; Belli, C.; Zaldei, A.; Bianconi, R.; and Gioli, B. 2015. Intercomparison of UAV, aircraft and satellite remote sensing platforms for precision viticulture. *Remote Sensing*, 7(3): 2971–2990.
- Mnih, V.; and Hinton, G. E. 2012. Learning to label aerial images from noisy data. In *Proceedings of the 29th International conference on machine learning (ICML-12)*, 567–574.
- Niethammer, U.; James, M.; Rothmund, S.; Travelletti, J.; and Joswig, M. 2012. UAV-based remote sensing of the Super-Sauze landslide: Evaluation and results. *Engineering Geology*, 128: 2–11.
- Noroozi, M.; and Favaro, P. 2016. Unsupervised learning of visual representations by solving jigsaw puzzles. In *European conference on computer vision*, 69–84. Springer.
- Ozesmi, S. L.; and Bauer, M. E. 2002. Satellite remote sensing of wetlands. *Wetlands ecology and management*, 10(5): 381–402.
- Pajares, G. 2015. Overview and current status of remote sensing applications based on unmanned aerial vehicles (UAVs). *Photogrammetric Engineering & Remote Sensing*, 81(4): 281–330.
- Parcak, S. H. 2009. *Satellite remote sensing for archaeology*. Routledge.
- Parcak, S. H. 2019. *Archaeology from Space: How the Future Shapes Our Past*. Henry Holt and Co., illustrated edition edition.
- Salamí, E.; Barrado, C.; and Pastor, E. 2014. UAV flight experiments applied to the remote sensing of vegetated areas. *Remote Sensing*, 6(11): 11051–11081.
- Schowengerdt, R. A. 2006. *Remote sensing: models and methods for image processing*. Elsevier.
- Tian, Y.; Sun, C.; Poole, B.; Krishnan, D.; Schmid, C.; and Isola, P. 2020. What makes for good views for contrastive learning? *arXiv preprint arXiv:2005.10243*.
- Tucker, C. J.; and Sellers, P. 1986. Satellite remote sensing of primary production. *International journal of remote sensing*, 7(11): 1395–1416.
- Verbyla, D. L. 1995. *Satellite remote sensing of natural resources*, volume 4. CRC Press.
- Wu, Z.; Xiong, Y.; Yu, S. X.; and Lin, D. 2018. Unsupervised feature learning via non-parametric instance discrimination. In *Proceedings of the IEEE conference on computer vision and pattern recognition*, 3733–3742.
- Zhuang, C.; Zhai, A. L.; and Yamins, D. 2019. Local aggregation for unsupervised learning of visual embeddings. In *Proceedings of the IEEE/CVF International Conference on Computer Vision*, 6002–6012.